

Photoconductivity in BiFeO₃ thin films

S. R. Basu,^{1,2} L. W. Martin,^{1,2,a)} Y. H. Chu,^{1,2} M. Gajek,^{1,2} R. Ramesh,^{1,2} R. C. Rai,^{3,b)} X. Xu,³ and J. L. Musfeldt³

¹Departments of Materials Science and Engineering and Physics, University of California-Berkeley, Berkeley, California 94720, USA

²Materials Science Division, Lawrence Berkeley National Laboratory, Berkeley, California 94720, USA

³Department of Chemistry, University of Tennessee, Knoxville, Tennessee 37996, USA

(Received 14 November 2007; accepted 4 February 2008; published online 4 March 2008)

The optical properties of epitaxial BiFeO₃ thin films have been characterized in the visible range. Variable temperature spectra show an absorption onset near 2.17 eV, a direct gap (2.667 ± 0.005 eV at 300 K), and charge transfer excitations at higher energy. Additionally, we report photoconductivity in BiFeO₃ films under illumination from a 100 mW/cm² white light source. A direct correlation is observed between the magnitude of the photoconductivity and postgrowth cooling pressure. Dark conductivities increased by an order of magnitude when comparing films cooled in 760 and 0.1 Torr. Large increases in photoconductivity are observed in light. © 2008 American Institute of Physics. [DOI: 10.1063/1.2887908]

In recent years, multiferroic materials have attracted attention due to the potential for development of memory devices based on the magnetoelectric effect.¹ One highly studied multiferroic material is BiFeO₃ (BFO).² Thin films of the rhombohedrally distorted perovskite BFO have been shown to have robust ferroelectricity with a saturation polarization of ~ 90 $\mu\text{C}/\text{cm}^2$ and an out-of-plane piezoelectric coefficient (d_{33}) of ~ 70 pm/V.² BFO is also known to be a canted *G*-type antiferromagnetic with a weak ferromagnetic moment of 8–10 emu/cm.³ Much of the interest concerning BFO stems from the high ordering temperatures in this material [ferroelectric Curie temperature (T_C) ~ 1103 K (Ref. 4) and Néel temperature (T_N) ~ 643 K (Ref. 5)] which makes it a suitable material for high-temperature applications. The optical properties of BFO, however, have remained relatively unexplored.

Although there is little experimental data concerning the optical properties of BFO, a number of recent theoretical studies have begun to focus on this subject. Such studies have predicted the band gap of BFO to have values that are within or near the visible range.^{6,7} Neaton *et al.* studied the spontaneous polarization in BFO using LSDA+U techniques and extracted a band gap in the near-visible range—approximately 1.9 eV.⁶ More recently, Clark and Robertson employed the screened-exchange density functional theory approximation to estimate the band gap of BFO—their calculation yielded a band gap of approximately 2.8 eV.⁷ Both approximations yielded a slightly indirect band gap. In addition to calculations placing the band gap of BFO in or near the visible range, BFO has the added intriguing possibility that it might possess an anomalous photovoltaic effect. Since the 1960s, the anomalous photovoltaic effect has been observed in a number of ferroelectric materials and the effect has been characterized in detail.⁸ For photovoltaic ferroelectrics, it has been observed that a homogeneous short-circuited crystal displays a photocurrent in the direction of spontaneous polarization under uniform illumination. The nonequilibrium photoexcited carriers are effectively driven

by the ferroelectric polarization. Finally, the ability to tune the oxidation state of the Fe ion in BFO may enable researchers to engineer the band gap and conductivity to enhance the photoferroelectric properties. The possibility of exciton creation in BFO under the visible spectrum not only implies its potential as a photovoltaic material but also suggests the development of a host of optoelectronic devices involving BFO's unique optical and multiferroic properties, thus motivating the current study.

Thin films of BFO between 100–500 nm thick were deposited on 50 nm thick films of the bottom electrode SrRuO₃ (SRO) on SrTiO₃ (STO) (111), bare STO (111), and DyScO₃ (DSO) (110) substrates. BFO films were deposited at 700 °C in 100 mTorr partial pressure of oxygen and then cooled in a range of partial pressures of oxygen from 0.01–760 Torr with the purpose of tuning the oxygen stoichiometry. Asymmetric [Sn-doped In₂O₃ (ITO) (~ 300 nm)/BFO/SRO] thin film devices with 54 μm diameter top contacts were also produced to study current-voltage (*IV*) characteristics in these films.

X-ray diffraction (XRD) [Fig. 1(a)] reveals high quality, epitaxial films that appear to be single phase regardless of the cooling pressure. The inset figure shows a detailed look at the pseudocubic-222 diffraction peaks of the different BFO/SRO/STO (111) heterostructures. No noticeable shift of the BFO 222 diffraction peak is observed with varying cooling pressure, pointing to the ability to tune oxygen stoichiometry without greatly affecting the BFO structure. We have also investigated the ferroelectric properties of these BFO films using a combination of atomic force microscopy (AFM), piezoresponse FM (PFM), and polarization-electric field (*P-E*) hysteresis loop measurements. AFM imaging [Fig. 1(b)] of the 760 and 0.1 Torr cooled BFO films reveals very smooth films—average rms roughness of 1.05 nm—with atomic terraces present even at film thicknesses greater than 250 nm. AFM images of samples cooled at 0.01 Torr, however, indicate the onset of surface second-phase formation, likely due to Bi loss. The volume fraction of second-phase is expected to be negligible, as no clearly identifiable second-phase peak was present in the XRD θ - 2θ scans and we believe the second phase is confined to the surface of the films. Additionally, PFM was used to probe the

^{a)}Electronic mail: lwmartin@berkeley.edu.

^{b)}Current address: Physics Department, Buffalo State College, New York 14222.

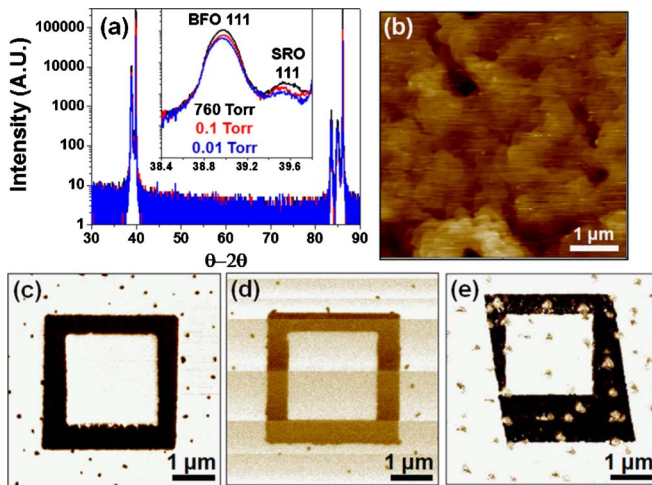


FIG. 1. (Color online) Structural and ferroelectric characterization of (111)-oriented BFO/SRO/STO heterostructures. (a) θ - 2θ XRD scan. (b) Typical AFM image of BFO/SRO/STO (111) films (z scale height of 10 nm). Out-of-plane PFM images demonstrating switching of films cooled in (c) 760 Torr, (d) 0.1 Torr, and (e) 0.01 Torr partial pressure of oxygen.

ferroelectric nature of the films. By applying a voltage to the tip during the scan, we were able to reversibly switch the polarization for all films regardless of cooling pressure [Figs. 1(c)–1(e)]. Polarization in BFO is oriented along the $\langle 111 \rangle$ body diagonals. As a result, in a (111)-oriented film, polarization can either point down toward the bottom electrode (imaged as white contrast in the out-of-plane PFM image) or up (imaged as black), with no in-plane component. Films used in this experiment were almost entirely downward polarized in the as-grown state with the exception of small upward pointing domains that form due to electrostatic relaxation in these relatively thick films. Furthermore, the selection of (111)-oriented films ensures that the maximum photoferroelectric driving force is present during the measurements. P - E hysteresis loop measurements revealed high quality, square hysteresis loops with a saturation polarization of $\sim 90 \mu\text{C}/\text{cm}^2$ for all films (data not shown).

Optical transmittance measurements were used to probe the electronic structure of BFO. These experiments were performed using a Perkin Elmer Lambda-900 spectrometer (3000–190 nm, 0.41–6.53 eV) between 4 and 730 K in BFO films grown on DSO (110) substrates. The wide band gap of DSO allowed us to probe the electronic structure of BFO up to 5 eV in 100 nm thick films. The absorption spectrum [Fig. 2(a)] displays two features centered at 3.2 and 4.5 eV that are assigned as charge transfer excitations, as suggested by the calculated electronic structure.^{8,9} We also observe a small shoulder centered at 2.5 eV in the 4 K spectrum.

It is well known that the absorption coefficient, $\alpha(E)$, in solids consists of contributions from both the direct and the indirect band gap transitions,⁹ and is given by

$$\alpha(E) = \frac{A}{E}(E - E_{g,\text{dir}})^{0.5} + \frac{B}{E}(E - E_{g,\text{ind}} \mp E_{\text{ph}})^2, \quad (1)$$

where $E_{g,\text{dir}}$ and $E_{g,\text{ind}}$ are the magnitudes of direct and indirect gaps, respectively, E_{ph} is the emitted (absorbed) phonon energy, and A and B are constants. This model, while assuming a simple band shape, allows for extraction of the direct energy gap by plotting $\alpha(E)^2$ as a function of photon energy.

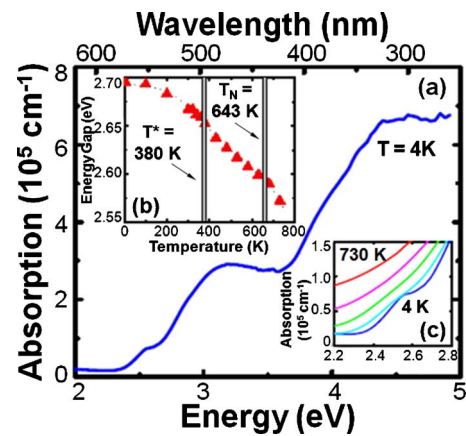


FIG. 2. (Color online) (a) Optical absorption of a 100 nm (111) oriented BFO film on DSO substrate at 4 K. (b) Energy gap as a function of temperature, determined from a direct gap analysis. Vertical lines denote transition temperatures ($T_N=643$ K, $T^*=380$ K). Error bars are on the order of the symbol size. (c) Close-up view of the shoulder at 2.5 eV. The 4, 300, 430, 580, and 730 K data are shown.

Linear extrapolation of $\alpha(E)^2$ to zero yields a gap of 2.695 ± 0.005 eV at 4 K and 2.667 ± 0.005 eV at 300 K. Plotting $\alpha(E)^{0.5}$ as a function of energy yielded a poor fit with no evidence for emitted/absorbed phonons, suggesting that BFO is a direct gap material. Figure 2(b) shows the temperature dependence of the gap. The overall redshift is consistent with the work of Tabares–Munos *et al.* for a strong negative shift ($-5.9 \text{ cm}^{-1} \text{ K}^{-1}$) of the absorption edge with temperature that turns BFO opaque upon heating.¹⁰ At the same time, the gap softens significantly through both T_N and $T^*=380$ K, the latter of which correlates with second harmonic generation effects observed in similar films.¹¹ The leading edge of the ~ 2.5 eV shoulder represents the onset to the optical absorption (at ~ 2.17 eV at 300 K). At this time, we cannot discern whether the shoulder is simply a low-lying feature of the electronic structure or whether it is evidence for excitonic character.

Dark-light IV characteristics were measured to investigate if a change in conductivity appeared under illumination. The resulting current of photoexcited carriers, driven by the intrinsic polarization, can be described by the following equation:

$$J = (\sigma_d + \sigma_{\text{ph}})\xi, \quad (2)$$

which is typical of photoferroelectric materials.¹⁰ σ_d and σ_{ph} represent the dark and light components of the conductivity, respectively. Under illumination in light of wavelength equal to or larger than the band gap the photoconductivity will effectively “turn on” and a larger current should be measured at all applied fields. A 100 mW/cm² white light peaked around ~ 550 nm was chosen as an appropriate source to test for photoexcitation given that both theoretical calculations and absorption/transmission spectra suggest that the band gap of BFO lies in the visible/near-visible range. Preliminary results indicated a jump in conductivity under illumination at nonzero applied fields only for through-film pathways with resistance of $< \sim 10 \text{ M}\Omega$. Noting that large leakage currents in BFO have typically been attributed to the presence of oxygen vacancies,¹² we proceeded to investigate a series of samples grown at 700 °C and 100 mTorr partial pressure of O₂ and then cooled to room temperature at varying pressures

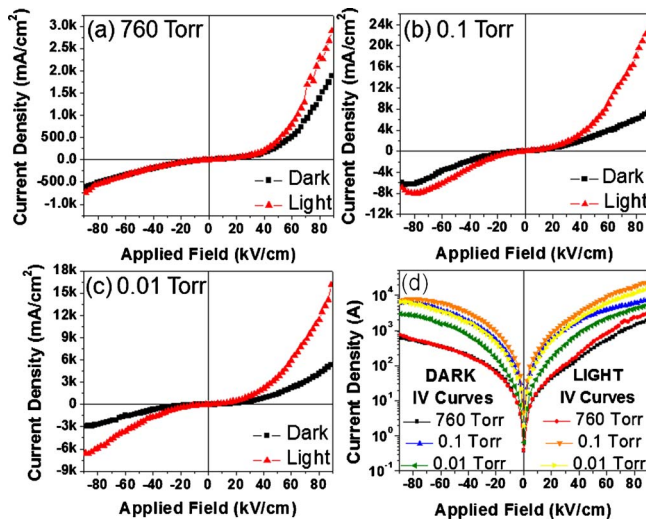
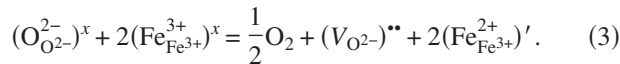


FIG. 3. (Color online) Light and dark current density as a function of applied field for BFO/SRO/STO (111) films cooled at (a) 760 Torr, (b) 0.1 Torr, and (c) 0.001 Torr partial pressure of oxygen. (d) Log current density for the data shown in (a)–(c).

in order to control the oxygen stoichiometry. The presence of oxygen vacancies effectively introduces electrons into the lattice and increases the free-carrier concentration. It should also be noted that a significant color change in samples cooled at varying oxygen pressures was observed, suggesting a shift of the absorption edge with changing oxygen stoichiometry. This is consistent with theoretical predictions of the introduction of interband states upon transformation of Fe^{3+} to Fe^{2+} in the lattice.¹³ The defect chemistry in BFO can be expressed using Kröger–Vink notation as



Electrons can then hop from Fe^{2+} to adjacent Fe^{3+} ions through oxygen centers. In support of this theory, Pabst *et al.* recently identified Poole–Frenkel conduction as being the dominant leakage mechanism in BFO thin films.¹⁴

Figure 3 shows both dark and light *IV* characteristics of 225 nm thick BFO films. Figures 3(a)–3(c) refer to dark and light *IV* curves taken on samples cooled in 760, 0.1, and 0.01 Torr, respectively. At an applied field of 60 kV/cm, dark conductivities of 8.58×10^{-6} , 6.48×10^{-5} , and $3.68 \times 10^{-5} \Omega^{-1} \text{cm}^{-1}$ were measured for samples cooled at 760 Torr [Fig. 3(a)], 0.1 Torr [Fig. 3(b)], and 0.01 Torr [Fig. 3(c)], respectively. Illuminated conductivities of 1.34×10^{-5} , 1.51×10^{-4} , and $9.90 \times 10^{-5} \Omega^{-1} \text{cm}^{-1}$ were measured for samples cooled at 760 Torr [Fig. 3(a)], 0.1 Torr [Fig. 3(b)], and 0.01 Torr [Fig. 3(c)], respectively. Nearly symmetric dark *IV* behavior [Fig. 3(d)] indicates that the change in conductivity upon illumination is not simply the result of excitation across a Schottky barrier with either contact. To rule out the possibility that the effect observed arose from excitation of carriers across the Schottky barrier between ITO and BFO, we explored symmetric ITO/SRO (2 nm)/BFO/SRO devices, where it is believed that SRO should make Ohmic contact with the BFO film.¹⁴ The *IV* behavior of the symmetric devices showed similar differences between light and dark *IV* measurements, confirming that photoresponse is intrinsic to the BFO (data not shown). We have also included light conductivity data in Fig. 3(d) to

further illustrate the differences between the different cooling processes.

The data suggest that the best photoresponse is demonstrated by samples cooled in partial pressure of oxygen at or less than 0.1 Torr, where we have observed conductivities that double upon illumination and are over an order of magnitude greater than those observed in fully oxidized samples. It was further observed that upon application of the external field in the same direction as the intrinsic polarization (i.e., positive in Fig. 3), the measured change in conductivity was greater in all samples. These findings are consistent with the model present in Eq. (2) and serve as further evidence of the photoferroelectric effect in BFO.

In summary, we have confirmed theoretical predictions that BFO not only possesses a band gap in the visible range but also that it displays a significant photoresponse which improves with increasing oxygen vacancy concentration. To date, however, we have not observed any diode behavior in our BFO heterostructures which could be a result of diminished capacitance in reduced films. As has been observed in bulk photoferroelectrics, the increase in conductivity under illumination is greater at applied fields coincident with the direction of spontaneous polarization in our BFO thin films. Although our reduced films display anomalously large photocurrents, photovoltages are very small. We aim to investigate a number of potential contact materials in order to improve the photoconductive properties of BFO and render it exploitable for optoelectronic devices. In addition, we also aim to conduct a more rigorous investigation of the relation of oxygen vacancy chemistry and photoconductivity.

At Berkeley, this work was performed within the Helios Solar Energy Research Center which is supported by the Director, Office of Science, Office of Basic Energy Sciences, Materials Sciences and Engineering Division, of the U.S. Department of Energy under Contract No. DE-AC02-05CH11231. At University of Tennessee, the research was supported by the Materials Science Division, Basic Energy Sciences, U.S. Department of Energy (DE-FG02-01ER45885). We also acknowledge Cyrus Wadia, Yue Wu, and Professor Paul Alivisatos for use of their facilities.

¹M. Fiebig, T. Lottermoser, D. Frohlich, A. V. Goltsev, and R. V. Pisarev, *Nature (London)* **419**, 818 (2002).

²J. Wang, J. B. Neaton, H. Zheng, V. Nagarajan, S. B. Ogale, B. Liu, D. Viehland, V. Vaithyanathan, D. G. Schlom, U. V. Waghmare, N. A. Spaldin, K. M. Rabe, M. Wuttig, and R. Ramesh, *Science* **299**, 1719 (2003).

³C. Ederer and N. Spaldin, *Phys. Rev. B* **71**, 060401 (2005).

⁴S. V. Kisilev, R. P. Ozerov, and G. S. Zhdanov, *Sov. Phys. Dokl.* **7**, 742 (1963).

⁵J. R. Teague and R. Gerson, *Solid State Commun.* **8**, 1073 (1970).

⁶J. B. Neaton, C. Ederer, U. V. Waghmare, N. A. Spaldin, and K. M. Rabe, *Phys. Rev. B* **71**, 014113 (2005).

⁷S. J. Clark and J. Robertson, *Appl. Phys. Lett.* **90**, 132903 (2007).

⁸V. Fridkin, *Photoferroelectrics* (Springer, New York, 1979).

⁹J. I. Pankove, *Optical Processes in Semiconductors* (Dover, New York, 1971).

¹⁰C. Tabares-Munos, J.-P. Rivera, and H. Schmid, *Ferroelectrics* **55**, 235 (1984).

¹¹A. Kumar, R. C. Rai, N. J. Podraza, S. Denev, M. Ramirez, Y. H. Chu, L. W. Martin, J. Ihlefeld, T. Heeg, J. Schubert, D. G. Schlom, J. Orenstein, R. Ramesh, R. W. Collins, J. L. Musfeldt, and V. Gopalan, *Appl. Phys. Lett.* (submitted).

¹²Y. P. Wang, L. Zhou, M. F. Zhang, X. Y. Chen, J. M. Liu, and Z. G. Liu, *Appl. Phys. Lett.* **84**, 1731 (2004).

¹³C. Ederer and N. Spaldin, *Phys. Rev. B* **71**, 224103 (2005).

¹⁴G. W. Pabst, L. W. Martin, Y. H. Chu, and R. Ramesh, *Appl. Phys. Lett.* **90**, 072902 (2007).